ChemPubSoc Europe

DOI: 10.1002/cmdc.201600528

CHEMMEDCHEM Full Papers

Potent and Selective Non-hydroxamate Histone Deacetylase 8 Inhibitors

Alexander Kleinschek,[a] Christian Meyners,[a] Eros Digiorgio,[b] Claudio Brancolini,[b] and Franz-Josef Meyer-Almes*[a]

Specific inhibition of histone deacetylase 8 (HDAC8) has been suggested as a promising option for the treatment of neuroblastoma and T-cell malignancies. A novel class of highly potent and selective HDAC8 inhibitors with a pyrimido[1,2-*c*][1,3]benzothiazin-6-imine scaffold was studied that is completely different from the traditional concept of HDAC inhibitors comprising a zinc binding group (ZBG), in most cases a hydroxamate group, a spacer, and a capping group that may interact with the surface of the target protein. Although lacking a ZBG, some of the new compounds were shown to have outstanding potency against HDAC8 in the single-digit nanomolar range. The pyrimido[1,2-*c*][1,3]benzothiazin-6-imines also inhibited the growth of solid and hematological tumor cells. The small size and beneficial physicochemical properties of the novel HDAC inhibitor class underline the high degree of drug likeness. This and the broad structure–activity relationship suggest great potential for the further development of compounds with the pyrimido[1,2-*c*][1,3]benzothiazin-6-imine scaffold into innovative and highly effective therapeutic drugs against cancer.

Introduction

Histone deacetylases (HDACs) are important regulators of gene expression. Together with histone acetyl transferases (HATs), HDACs control not only the acetylation status of histones but also other lysine-acetylated cellular proteins comprising approximately 5–10% of the proteome, also called the K-acetylome, of species from bacteria to humans.[1] The HDACs are divided in four major classes with respect to sequence similarity. Class I (HDACs 1–3, 8), class II (HDACs 4–7, 9, 10), and class IV (HDAC 11) contain zinc-dependent enzymes, whereas class III enzymes (sirtuins 1–7) are NAD^+-dependent lysine deacetylases. Owing to their important role in transcriptional regulation, it is not surprising that aberrant activity can cause serious disorders. Several studies clearly identified HDAC8 to be involved in various cancer diseases, such as T-cell lymphoma[2] and neuroblastoma,[3] and is overexpressed in urothelial[4] and breast cancer.[5] Very recently, Oehme et al. demonstrated the benefit of selective inhibition of HDAC8 in two xenograft neuroblastoma mouse models.[6] The selective HDAC8 inhibitors showed antitumor activity without side effects, whereas the pan-HDAC inhibitor vorinostat was clearly more toxic. Despite these promising results, no active substance specifically targeted at HDAC8 has found its way into clinics.

The principal structural concept of all known inhibitors of zinc-dependent HDACs comprises a zinc binding group (ZBG) for the recognition of the catalytic zinc ion, a spacer mimicking the lysine residue, and a capping group to increase the selectivity of the isoforms due to interaction with specific residues at the rim of the binding pocket. Typical examples of unselective HDAC inhibitors are shown in Figure 1a, including **1** (vorinostat), **2** (romidepsin), **3** (belinostat), and **4** (panabinostat), which have been approved by the FDA for the treatment of cutaneous T-cell lymphoma or multiple myeloma. Actually, more than 10 HDAC inhibitors, most of them bearing a hydroxamate group, are in clinical trials.[7] The hydroxamic acid ZBG confers high affinity to these inhibitors because of its extraordinary capability to tightly coordinate to the catalytic zinc ion at the bottom of the binding pocket. However, the metal-complexing feature of hydroxamic acids raises some concerns regarding unselective inhibition of other HDAC isoforms or other metal-dependent enzymes such as matrix metalloproteinases (MMPs). For example, more than 50 hydroxamic acids and inhibitors of MMPs have been taken forward to clinical trials as potential anticancer drugs, but all of them failed owing to lack of specificity, metabolic instability, toxicity, or insufficient knowledge of how the MMPs were linked to the disease.[8] On the other hand, in some cases, remarkable isoform selectivity of hydroxamic acids has been achieved by optimized capping groups interacting with specific regions on the surface of the target enzyme. Known selective HDAC8 inhibitors are shown in Figure 1b and include linkerless hydroxamic acids **5** (A8B4),[9] **6** (PCI-34051),[2] and **9**[10] as well as non-hydroxamates **7** and **8**.[11]

[a] *A. Kleinschek, C. Meyners, Prof. Dr. F.-J. Meyer-Almes*
Department of Chemical Engineering and Biotechnology, University of-Applied Sciences, Schnittspahnstr. 12, 64287 Darmstadt (Germany)
E-mail: franz-josef.meyer-almes@h-da.de

[b] *E. Digiorgio, Prof. Dr. C. Brancolini*
Dipartimento di Scienze Mediche e Biologiche, MATI Center of Excellence, Università degli Studi di Udine, P.le Kolbe 4, 33100 Udine (Italy)

Supporting Information (synthetic details, physical and spectral data of synthesized compounds, dose–response curves of all synthesized compounds against HDAC8, summary of all IC_{50} values for the thione intermediates, and LC–MS data demonstrating the chemical stability of **13a** under the applied biochemical assay conditions) and the ORCID identification number(s) for the author(s) of this article can be found under http://dx.doi.org/10.1002/cmdc.201600528.

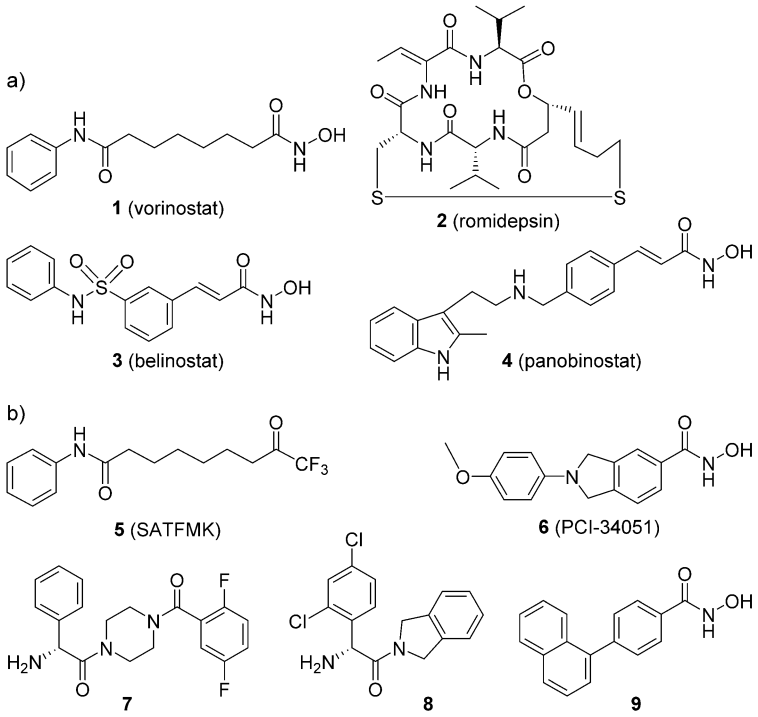

Figure 1. Known HDAC inhibitors: a) approved cancer drugs and b) HDAC8-selective inhibitors.

In addition to the inherent selectivity problems of compounds with hydroxamate functional groups, there are also experimental findings pointing to mutagenic effects[12] that may not prohibit the use of a hydroxamic acid drug against a life-threatening disease such as cancer, for which some side effects may be acceptable, but compromise a chronic application in other medical indications such as neurological disorders, as discussed very recently by Shen and Kozikowski.[13] Currently, the identification and development of potent, selective, and drug-like HDAC inhibitors lacking the problematic hydroxamate group remains a challenging area.

Results and Discussion

Chemistry

In a screen of the Library of Pharmacologically Active Compounds (LOPAC) against HDAC8, we identified and confirmed **13a** (PD-404,182) as a potent hit. The LOPAC library contains a collection of 1280 pharmacologically active compounds with known targets and modes of action. Compound **13a** has been claimed as both an antiviral[14] and an antibacterial agent[15] but has never been suggested as a HDAC inhibitor. Moreover, we found a striking selectivity against HDAC8 upon testing a panel of HDAC isoforms (Table 1).

The chemical structure of **13a** deviates entirely from that of traditional HDAC inhibitors consisting of a ZBG, linker, and capping group. In fact, no zinc chelating group is present in this low-molecular-weight compound. The beneficial physicochemical and pharmacological properties of **13a** with respect to Lipinski rules[16] (no violation), solubility [log *D* (pH 7.4) = 2.09], cell permeability [polar surface area (PSA) = 65 Å^2], ligand efficiency[17] (LE = 2.88 kJ mol^{-1}), and lipophilic efficiency[18] (LIPE = 5.5) make this compound an ideal starting point for the development of next-generation HDAC8 inhibitors with druglike properties. To establish structure–activity as well as structure–selectivity relationships, a small collection of derivatives of **13a** was designed and synthesized. We explored the influence of variation in the substituents of the aryl ring and the ring size of the nitrogen heterocycle on the activity against a panel of HDAC isoforms. Intermediate thiones **12a–m** were also tested to assess the importance of the imine group but were found to be 35 to 1000 times less active against HDAC8. The synthetic route toward the pyrimido[1,2-*c*][1,3]benzothiazin-6-imines (*n* = 3) and imidazo[1,2-*c*][1,3]benzothiazin-6-imines (*n* = 2) is described in Scheme 1 and essentially followed the procedure of Mizuhara et al.[14b,19] Some compounds (i.e., **13c**, **13e**, **13h**, **13i**, **13l**, and **13m**) were synthesized and tested for the first time.

Biochemical in vitro assays

To assess the potency and selectivity of the synthesized compounds, standardized enzyme activity assays were performed against zinc-dependent human HDACs 1–8 by using fluorogenic acetylated lysine substrates (see Figure 2 and Figure S1 in Supporting Information). The calculated IC_{50} values are summarized in Table 1. For comparison purposes, activity data of known HDAC8 inhibitors are added. The imines are able to inhibit HDAC8 down to single-digit nanomolar IC_{50} values, which underlines the great potential for further optimization of these compounds. Surprisingly, this very high potency is achieved by

Table 1. Selectivity profile of 3,4-dihydrobenzo[*e*]pyrimido[1,2-*c*][1,3]thiazin-6(2*H*)-imine and 2*H*-benzo[*e*]imidazo[1,2-*c*][1,3]thiazin-5(3*H*)-imine against selected HDAC isoforms.

Compd	IC_{50} [μM]							
	HDAC1	HDAC2	HDAC3	HDAC4	HDAC5	HDAC6	HDAC7	HDAC8
13a	3.6±0.8	32±1.5	>50	8.6±1.5	0.11±0.01	6.7±0.8	0.22±0.02	0.011±0.001
13b	>50	>50	>50	>50	>50	>50	1.3±0.71	4.4±0.8
13c	21±1	>50	>50	>50	13±1	32±18	0.5±0.2	0.18±0.02
13d	34±2	>50	>50	>50	12±1	14±1	2.0±0.5	0.072±0.003
13e	7.9±0.2	>50	20±1	5.7±0.3	1.0±0.1	1.2±0.4	0.08±0.02	0.0059±0.0003
13f	2.9±0.3	>50	10±0.56	2.84±0.13	0.17±0.02	9.0±4.0	2.6±0.4	0.0041±0.0002
13g	1.7±0.2	>50	6.7±0.4	2.0±0.1	0.14±0.02	2.8±0.7	1.7±0.2	0.0029±0.0001
13h	35±3	>50	>50	5.1±0.6	0.74±0.16	5.2±1.1	5±1	0.017±0.001
13i	>50	>50	>50	>50	>50	>50	>50	9.2±0.3
13j	2.6±0.3	16±2	7.0±0.5	2.3±0.3	0.038±0.001	1.4±0.2	2.0±0.7	0.0063±0.0004
13k	5.8±0.3	>50	26±4	7.6±0.8	0.24±0.01	1.3±0.3	2.5±0.1	0.0054±0.0004
13l	2.1±0.2	30±2	5.3±0.4	2.2±0.3	0.046±0.003	0.65±0.11	1.5±0.4	0.0060±0.0006
13m	3.7±0.4	>50	9.6±0.7	3.2±0.5	0.038±0.002	1.3±0.3	1.3±0.2	0.0043±0.0005
12a	>50	>50	>50	>50	>50	>50	>50	2.8±0.3
12g	>50	>50	>50	>50	>50	>50	>50	0.6±0.1
12h	>50	>50	>50	>50	>50	>50	>50	13±1
12k	>50	>50	>50	>50	33±2	>50	>50	0.72±0.08
1	0.062±0.004	0.17±0.01	0.054±0.001	27±4	24±3	0.089±0.007	12±1	5.3±1.2
5	–	3.6[a]	–	–	–	15[a]	–	0.023[a]
6	3.0±0.2	45±13	38±3	10±1	>50	18±6	9.8±1.4	0.024±0.002
7	>30[b]	>30[b]	–	–	–	>30[b]	–	0.2[b]
8	1.7[b]	3.9[b]	–	–	–	>30[b]	–	0.09[b]
9	>100[c]	–	–	–	–	55[c]	–	0.3[c]

[a] Taken from Ref. [8]. [b] Taken from Ref. [10]. [c] Taken from Ref. [9]. Standard errors were calculated from nonlinear regression fit of a Hill model to 10 data points.

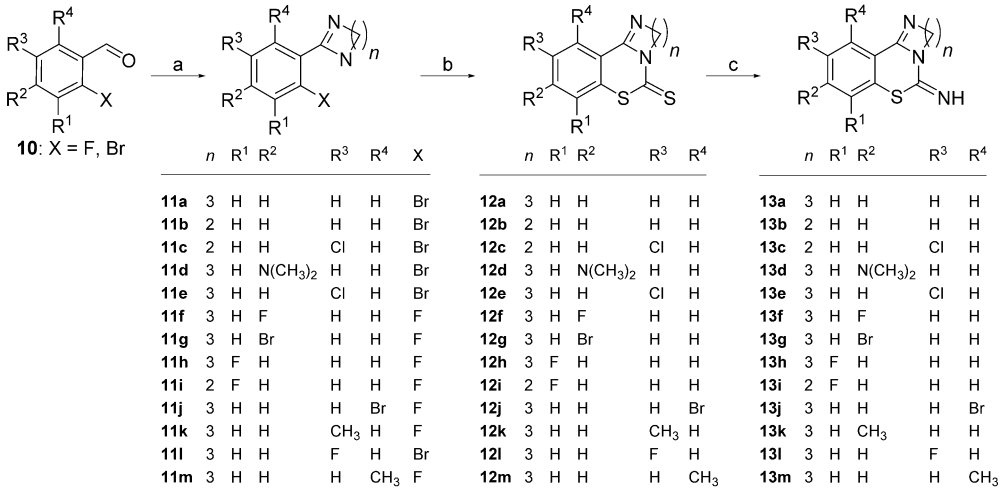

Scheme 1. Synthesis of pyrimido[1,2-*c*][1,3]benzothiazin-6-imines and imidazo[1,2-*c*][1,3]benzothiazin-6-imines for SAR studies: a) ethylene diamine or 1,3-diaminopropane, K_2CO_3, I_2; b) CS_2, NaH; c) 1. NaOH in MeOH/$H_2$0, 2. BrCN.

an absolutely exceptional chemical structure without a recognized ZBG. The imines are small and rather compact molecules with beneficial physicochemical properties and high ligand and lipophilicity efficiencies, which indicates a very high degree of drug likeness. Only known compounds **5**, **6**, and **8** show similar high potencies against HDAC8. However, the molecular weight and number of non-hydrogen atoms of **13a** are much lower than those of the known HDAC8 inhibitors, which enables more options for chemical optimization. In terms of the LE and LIPE of the imines, represented by **13a**, **13g** and **13h** appear to be clearly more druglike than compounds **7**, **8**, and **9** (see Table 2). Only **6** exhibits druglike features almost as good as those of the imine inhibitors. The test results of **13a**–**m** against the panel of HDAC isoforms revealed a remarkable correlation between potency against HDAC8 and selectivity against most HDACs with the exception of HDAC5 (Figure 3). This striking observation is in contrast to many other cases, for which the compounds of a series become more unselective

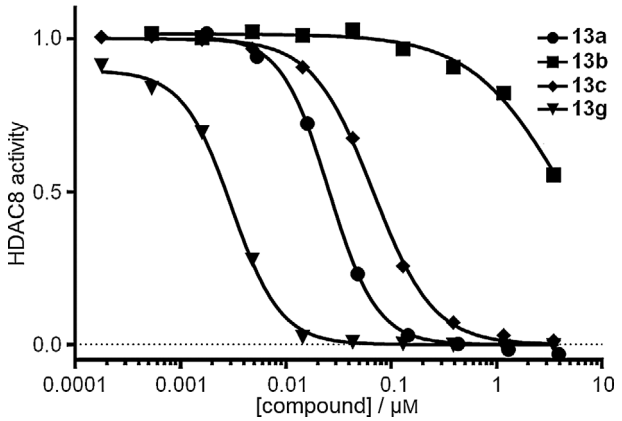

Figure 2. Dose–response curves of selected HDAC8 inhibitors.

Table 2. Physicochemical parameters to evaluate drug likeness.

Compd	M_r [Da]	$N^{[a]}$	log $D_{7.4}$[b]	LE [kJ mol^{-1}][c]	LIPE[d]
13a	217.3	15	2.09	2.88	5.5
13g	295.0	16	2.86	3.04	5.7
13h	235.3	16	2.24	2.77	4.9
5	568.2	42	3.98	1.04	3.7
6	284.1	21	2.24	2.17	5.7
7	407.1	28	1.86	1.36	4.8
8	334.1	22	2.77	1.83	4.3
9	263.3	20	3.46	1.86	4.7

[a] Number of non-hydrogen atoms. [b] Solubility partition coefficient between 1-octanol and water at pH 7.4. [c] Ligand efficiency. [d] Lipophilic efficiency.

with increasing potency. For our imine series, the optimization of potency seems to coincide with selectivity, which allowed the development of highly potent and selective HDAC8 inhibitors lacking a hydroxamate group. The distinctive correlation between selectivity and potency also suggests that the compounds recognize a particular site that is unique for HDAC8. Most known hydroxamate inhibitors are less potent against HDAC8 than the compounds of the imine series (Figure 3). Almost all hydroxamates are clearly less selective with respect to class I HDACs 1–3 and class IIb HDAC6 because of their pan-inhibitor properties. However, upon looking at selectivity against class IIa HDACs, the picture changes, because these enzymes are generally only weakly inhibited by hydroxamic acids. The most potent hydroxamic acids with regard to HDAC8 are LAQ824 and **6** (PCI-34051). Whereas LAQ824 is very unselective, PCI-34051 is highly selective against all other tested HDAC isoforms. However, several compounds of the imine series outperform the selectivity of PCI-34051 with respect to class I HDACs 1–3 and class IIb HDAC6. Moreover, as imine-based inhibitors **13a**–**m** are much smaller than PCI-34051, this allows lots of scope for the development of optimized inhibitors also with improved selectivity against class IIa HDACs. Okazaki et al. raised some concerns about the chemical stability of known antiviral agent **13a** and its derivatives.[20] They report that **13a** can undergo transformations to yield either a pyrimidothiazinone in the presence of DMSO/H_2O or a thiophenol under reductive conditions in the presence of glutathione (GSH). Given that the biochemical assay was performed under nonreductive conditions in the absence of a nucleophilic thiol-containing reagent, transformation into the corresponding thiophenol was not possible. For our biochemical assay, the compounds were freshly dissolved in water-free DMSO and then immediately serially diluted and tested for their capability to inhibit HDAC activity. The entire assay procedure was finished within 90 min. By using LC–MS experiments we could clearly demonstrate that **13a** remains essentially stable under our particular biochemical assay conditions and degrades to less than 4% within 2 h (see Figure S2).

Structure–activity relationships

The imine function is crucial for very strong inhibition of HDAC8, because corresponding thione intermediates **12a**–**m** were found to be substantially less potent against this enzyme (Table 1, Table S1, and Figure S1). Furthermore, the ring size of the nitrogen heterocycle had a tremendous impact on potency: as demonstrated by the direct comparison of three matching pairs of imine compounds (**13a**/**13b**, **13e**/**13c**, **13h**/**13i**), the 3,4-dihydrobenzo[e]pyrimido[1,2-c][1,3]thiazin-6(2*H*)-imines were at least 30 times more potent than the corresponding 2*H*-benzo[e]imidazo[1,2-c][1,3]thiazin-5(3*H*)-imines. Substitutions with halogen atoms or a methyl group were well tolerated at each aromatic position of lead compound **13a** and led to IC_{50} values in the single-digit nanomolar range. However, a dimethylamino group at the R^2 position was clearly disfavored and caused a strong drop in activity against the target enzyme. A principal component analysis (PCA) using 2D chemical descriptors of the thiazinimines is shown in Figure 4. The most potent compounds with single-digit nanomolar activity are grouped in a prolate cluster, which is highlighted by a black ellipsis in the center of the diagram. The PCA illustrates the large chemical space that is covered by diverse compounds with nanomolar potencies. This opens many opportunities to explore all aromatic positions of the thiazinimine pharmacophore and further optimize the potency of this compound class while preserving beneficial physicochemical parameters. On the basis of the observed correlation between potency and selectivity, we also expect an improvement in the selective recognition of HDAC8.

In vitro cell growth inhibition

To assess the effect of the thiazinimines on tumor cells, we tested three cell lines: two derived from solid tumors, SK-UT-1 (leiomyosarcoma) and MCF7 (breast cancer), and the Jurkat T-lymphocytes (acute T-cell leukemia). The data in Table 3 show that the compounds of the imine series inhibited human cancer cell lines in vitro with varying potencies. None of compounds **13a**–**m** was as effective against any of the tested cell lines as unselective reference compound **1**.

However, several imines were found to be more potent than HDAC8-selective reference compound **6**. Although no clear

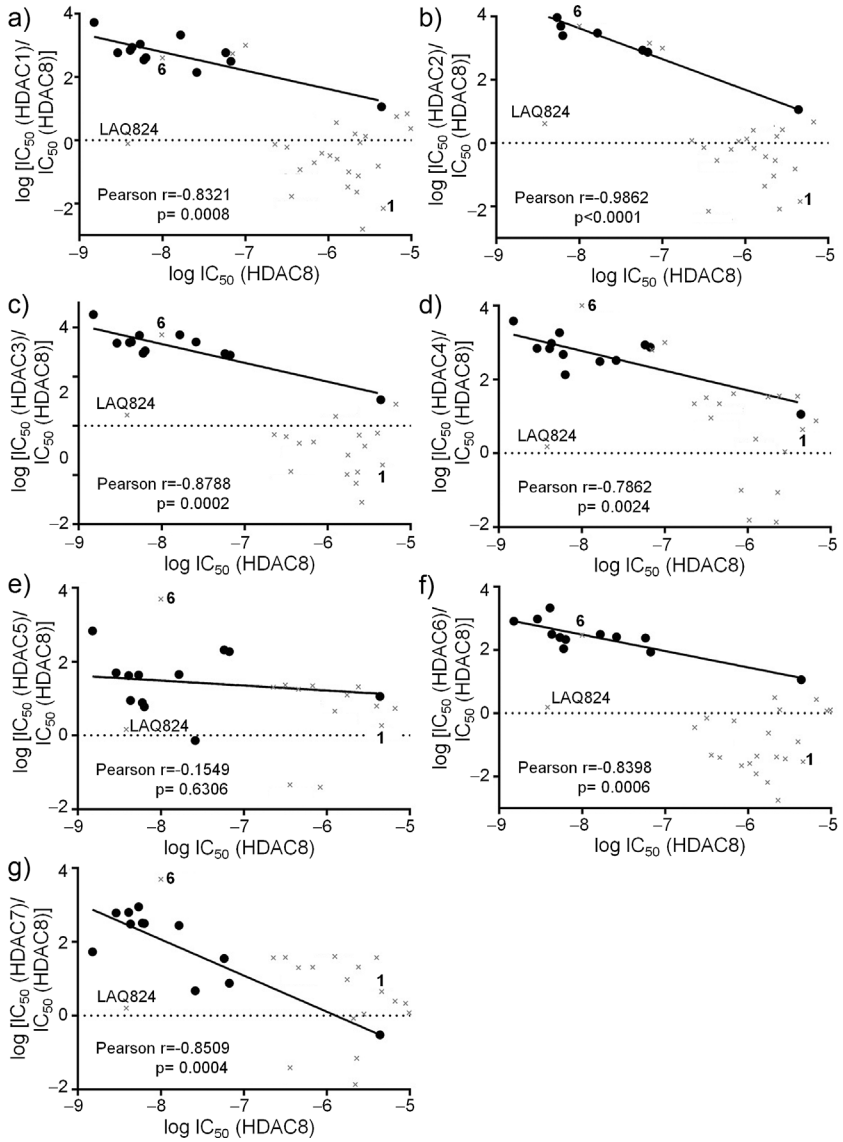

Figure 3. Selectivity of HDAC8 inhibitors versus a) HDAC1, b) HDAC2, c) HDAC3, d) HDAC4, e) HDAC5, f) HDAC6, and g) HDAC7. Black dots denote compounds of the imine series **13a**–**m**, and gray crosses represent hydroxamate inhibitors.

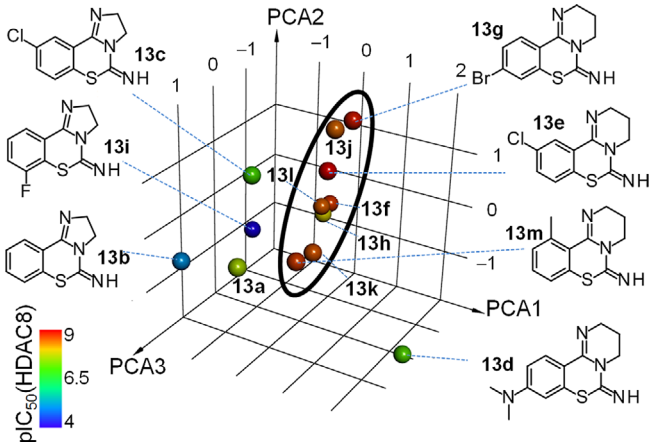

Figure 4. PCA of chemical descriptors characterizing compounds of the benzothiazinimine series. Each sphere represents one chemical entity labeled by its code number.

correlation between cell growth and HDAC8 inhibition could be observed, there was a trend that those compounds that were the most potent HDAC8 inhibitors also inhibited Jurkat cells more strongly (Figure 5). Compound **13i** with rather low biochemical activity differed completely from this tendency and showed unexpected high antiproliferative effects against Jurkat cells. With SK-UT-1 and MCF7 cells there was no correlation at all.

The investigation of Okazaki on **13a** showed that this compound was transformed into a thiophenol derivative under reductive conditions in the presence of GSH.[20] Therefore, the authors suggested that pyrimidobenzothiazine scaffolds may work as prodrug forms, and the bioactive substance within cells was believed to be at least partly the thiophenol derivative. With this knowledge, a correlation between the data of the biochemical assay with untransformed benzothiazin-6-imines and cell-based assay data cannot be expected at first

Table 3. Growth inhibition assay of human cancer cell lines.

Compound	GI_{50} [μM][a]		
	SK-UT-1	MCF7	Jurkat
13a	736±659	>1000	63±8
13b	343±191	213±50	558±342
13c	64±7	60±6	67±8
13d	106±21	200±58	153±28
13e	>1000	>1000	56±9
13f	147±73	>1000	33±3
13g	76±7	>1000	30±3
13h	>1000	>1000	42±3
13i	109±29	16±3	24±3
13j	16±3	11±3	17±3
13k	45±16	44±12	36±4
13l	24±5	79±11	16±2
13m	35±2	179±66	23±2
1 (SAHA)	5.4±0.4	3.7±0.4	3.7±0.4
6 (PCI-34051)	136±62	65±18	40±4

[a] Values are the mean±SEM, calculated from three independent experiments.

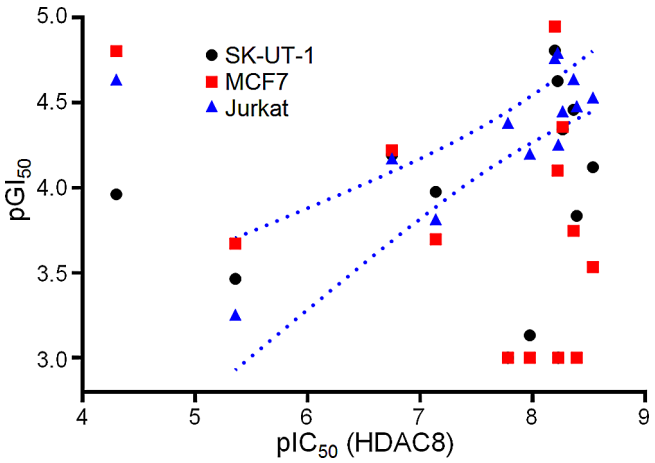

Figure 5. Growth inhibition of the three different cancer cell lines by compounds **13a**–**m**. Each data point represents an imine compound tested against the respective cell line. Blue dotted lines indicate the 95% confidence band of a linear regression fit (R^2=0.79, Pearson r=0.89) for the growth inhibition of Jurkat cells calculated under exclusion of the data point with lowest potency in the enzyme activity assay. The data for SK-UT-1 (Pearson r=0.24) and MCF7 (Pearson r=−0.066) are not significantly correlated with HDAC8 inhibition data.

glance. Balasubramanian et al. reported that **6** was selective for T-cells and much less cytotoxic to solid tumor cell lines.[2] We confirm this finding, but the differences between the growth inhibition of the T-cell line Jurkat and the solid tumor cell lines is not as pronounced as described in the previous study. Similar to **6**, multiple imines were more active on Jurkat cells than on SK-UT-1 or MCF7 cells, which suggests a similar mode of action. A number of imines were considerably more selective against Jurkat cells than **6** under identical assay conditions. The best selectivity was achieved with compound **13h**, which inhibited the growth of Jurkat cells more than 24 times more strongly than that of the SK-UT-1 and MCF7 cells, whereas **6** was only a factor of 3.6 and 1.7 more potent against Jurkat cells than the respective solid tumor cell lines. The growth inhibition experiments revealed that both potency and selectivity regarding cancer cells can be modulated by distinct substitutions at the aromatic ring of the thiazinimines.

Pyrimido[1,2-*c*][1,3]benzothiazin-6-imines increase SMC3 acetylation

Acetylated SMC3 is a validated substrate for HDAC8 in several human tumor cell lines.[21] Addition of **13a** and **13l** to Jurkat T-lymphocytes led to a significant increase in SMC3 acetylation after incubation for 3 h (Figure 6). This clearly demonstrated

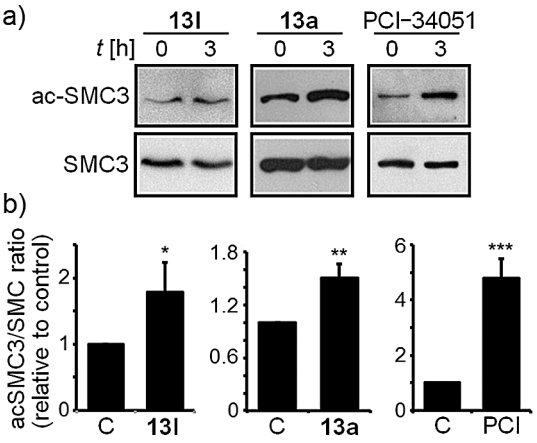

Figure 6. HDAC8 inhibition increases the acetylation levels of SMC3. a) Immunoblot analysis of acetylated SMC3 levels in Jurkat cells (5×10^5) treated for 3 h with the indicated HDAC inhibitors. Each compound was used at its GI_{50} concentration. b) Densitometric analysis of the acSMC3/SMC3 ratio in Jurkat cells treated as in panel (a); C=control; PCI=PCI-34051. Data are the mean±SEM of n=3 experiments; *$p<0.05$, **$p<0.01$, ***$p<0.005$.

that these compounds inhibited HDAC8 within living cells. However, the increase in SMC3 acetylation was much weaker than the effect of PCI-34051. As discussed above, this observation may be attributed to partial intracellular transformation or degradation of **13a** and **13l**. The underlying processes are currently being further investigated.

Conclusions

We discovered a novel class of potent and histone deacetylase 8 (HDAC8)-selective inhibitors based on the pyrimido[1,2-*c*][1,3]benzothiazin-6-imine chemical scaffold. The chemical structure of this new inhibitor class is completely different from that of traditional HDAC inhibitors, which comprises a zinc binding group (ZBG), in most cases a hydroxamate group, a spacer, and a capping group that may interact with the surface of the target protein. Although lacking a ZBG, some of the new compounds showed outstanding potency against HDAC8 in the single-digit nanomolar range. In addition, the selectivities obtained are similar to or better than those of the best-known HDAC8 inhibitors, and target engagement within Jurkat T-lymphocytes was confirmed. The excel-

lent potency and selectivity values were achieved with very small chemical structures and highly beneficial ligand efficiency and lipophilic efficiency physicochemical parameters, which suggests a high degree of drug likeness. The structure–activity relationship showed that there is still much room for further optimization of the pyrimido[1,2-*c*][1,3]benzothiazin-6-imines. Multiple derivatives show activity profiles regarding recombinant human HDAC isoforms and tumor cell lines that are very similar to those of reference compound **6**. However, it has to be clarified how and to which extent the pyrimido[1,2-*c*][1,3]benzothiazin-6-imines are transformed or degraded within living cells. Nevertheless, the promising results of this study and with selective HDAC8 inhibitors in xenograft mouse neuroblastoma models[6] make the pyrimido[1,2-*c*][1,3]benzothiazin-6-imines highly attractive non-hydroxamate alternatives in the treatment of neuroblastoma.

Experimental Section

Materials and methods

All of the starting materials were obtained commercially and were used without further purification. All of the reported yields are for isolated products and are not optimized. Nuclear magnetic resonance (^{1}H NMR and ^{13}C NMR) spectra were recorded with a Bruker DRX-500 spectrometer (operating at 500 MHz) with chemical shifts in parts per million (δ) downfield from tetramethylsilane, the internal standard. Mass spectrometry (MS) data were obtained by using an Agilent 6110 Quadrupole LC–MS system with a 0.3 mL min^{-1} flow rate by using a gradient mobile phase consisting of 0.1% trifluoroacetic acid (TFA) in water and 0.1% TFA in acetonitrile. UV detection was monitored at $\lambda = 227$ nm. Mass spectra were acquired either in positive or in negative mode scanning over the mass range of $m/z = 105$ to 1500. The purities of the final compounds were determined by using an Agilent 1200 series HPLC system by using a C-18 column (Waters Sunfire C_{18} 3.5 μm, 2.1 mm × 100 mm) and were found to be ≥95%. Flash column chromatography was conducted by using silica gel (Merck Kieselgel 60, No. 9385, 230–400 mesh ASTM). Gas chromatographic data were obtained by using an Agilent 7890A GC System (G3440A) with a mass detector VL MSD with Triple-Axis Detector (5975C) and an Agilent HP-5 MS column (19091S-433 30 m, 0.25 mm, 0.25 μm).

Synthesis

General procedure for the synthesis of 2-aryl-4,5-dihydro-1*H*-imidazoles 11 (*n* = 2) and 2-aryl-1,4,5,6-tetrahydropyrimidines 11 (*n* = 3): The diamine (1.1 equiv) was added to a solution of aldehyde **10** (1 equiv) in *tert*-butyl alcohol (9.0 mL mmol^{-1}), and the solution was stirred at 70 °C for 30 min. K_2CO_3 (4 equiv) and I_2 (1.25 equiv) were added at 70 °C, and the mixture was stirred at this temperature for another 3 h. The mixture was cooled down to RT, and $Na_2S_2O_3$ was added until the iodine color almost disappeared. The organic layer was separated, and the solvent was removed under reduced pressure. The received solid was dissolved in water (7.5 mL mmol^{-1}) and 2 N $NaOH_{(aq)}$ was added until pH 12–14. The aqueous layer was separated with $CHCl_3$ (3× 3.75 mL mmol^{-1}), the combined organic layer was dried (Na_2SO_4), and the solvent was removed under reduced pressure. The product was used without further purification.

2-(2-Bromophenyl)-1,4,5,6-tetrahydropyrimidine (11 a): White solid (970 mg, 47%).

2-(2-Bromophenyl)-4,5-dihydro-1*H*-imidazole (11 b): Orange oil (926 mg, 4.11 mmol, 82%).

2-(2-Bromo-5-chlorophenyl)-4,5-dihydro-1*H*-imidazole (11 c): Pale-yellow solid (876 mg, 3.38 mmol, 84%).

2-(2-Bromo-4-dimethylaminophenyl)-1,4,5,6-tetrahydropyrimidine (11 d): Brown solid (564 mg, 2.00 mmol, 99%).

2-(2-Bromo-5-chlorophenyl)-1,4,5,6-tetrahydropyrimidine (11 e): Yellow solid (992.7 mg, 3.63 mmol, 91%).

2-(2,4-Difluorophenyl)-1,4,5,6-tetrahydropyrimidine (11 f): Brown solid (1.73 g, 8.80 mmol, 88%).

2-(4-Bromo-2-fluorophenyl)-1,4,5,6-tetrahydropyrimidine (11 g): Brown solid (800 mg, 3.11 mmol, 12%).

2-(2,3-Difluorophenyl)-1,4,5,6-tetrahydropyrimidine (11 h): Brown solid (1.35 mg, 6.89 mmol, 69%).

2-(2,3-Difluorophenyl)-4,5-dihydro-1*H*-imidazole (11 i): Pale-yellow solid (1.55 g, 8.51 mmol, 85%).

2-(2-Bromo-6-fluorophenyl)-1,4,5,6-tetrahydropyrimidine (11 j): Pale-yellow solid (2.14 mg, 8.32 mmol, 83%).

2-(2-Fluoro-4-methylphenyl)-1,4,5,6-tetrahydropyrimidine (11 k): Brown viscous oil (1.93 mg, 10.0 mmol, quant.).

2-(2-Bromo-5-fluorophenyl)-1,4,5,6-tetrahydropyrimidine (11 l): Colorless solid (1.93 mg, 7.49 mmol, 75%).

2-(2-Fluoro-6-methylphenyl)-1,4,5,6-tetrahydropyrimidine (11 m): Pale-yellow solid (1.13 mg, 5.87 mmol, 80%).

2-(2-Fluoro-5-methylphenyl)-4,5-dihydro-1*H*-imidazole (11 n): Pale-yellow solid (1.71 g, 9.57 mmol, 96%).

General procedure for cyclization using carbon disulfide: CS_2 (2 equiv) was added to a mixture of **11** (1 equiv) and NaH (2 equiv) in DMF (3.3 mL mmol^{-1}) under a N_2 atmosphere. After stirring at 80 °C for 16 h, the mixture was concentrated under reduced pressure. The product was purified by chromatography.

3,4-Dihydrobenzo[*e*]pyrimido[1,2-*c*][1,3]thiazine-6(2*H*)-thione(12 a): Bright yellow solid (500 mg, 55%).

2*H*-Benzo[*e*]imidazo[1,2-*c*][1,3]thiazine-5(3*H*)-thione (12 b): Yellow crystals (156 mg, 61%).

9-Chloro-2*H*-benzo[*e*]imidazo[1,2-c][1,3]thiazine-5(3*H*)-thione (1 2c): Yellow crystals (360 mg, 71%).

9-(Dimethylamino)-3,4-dihydrobenzo[*e*]pyrimido[1,2-*c*][1,3]thiazine-6(2*H*)-thione (12 d): Yellow crystals (159 mg, 57%).

10-Chloro-3,4-dihydrobenzo[*e*]pyrimido[1,2-*c*][1,3]thiazine-6(2*H*)-thione (12 e): Yellow crystals (168 mg, 63%).

9-Fluoro-3,4-dihydrobenzo[*e*]pyrimido[1,2-*c*][1,3]thiazine-6(2*H*)-thione (12 f): Yellow crystals (656 mg, 65%).

9-Bromo-3,4-dihydrobenzo[*e*]pyrimido[1,2-*c*][1,3]thiazine-6(2*H*)-thione (12 g): Yellow crystals (578 mg, 47%).

8-Fluoro-3,4-dihydrobenzo[*e*]pyrimido[1,2-*c*][1,3]thiazine-6(2*H*)-thione (12 h): Yellow crystals (595 mg, 59%).

7-Fluoro-2*H*-benzo[*e*]imidazo[1,2-*c*][1,3]thiazine-5(3*H*)-thione (12 i): Yellow solid (727 mg, 76%).

11-Bromo-3,4-dihydrobenzo[*e*]pyrimido[1,2-*c*][1,3]thiazine-6(2*H*)-thione (12 j): Yellow crystals (210 mg, 17%).

9-Methyl-3,4-dihydrobenzo[*e*]pyrimido[1,2-*c*][1,3]thiazine-6(2*H*)-thione (12 k): Yellow crystals (323 mg, 33%).

10-Fluoro-3,4-dihydrobenzo[*e*]pyrimido[1,2-*c*][1,3]thiazine-6(2*H*)-thione (12 l): Yellow solid (482 mg, 48%).

11-Methyl-3,4-dihydrobenzo[*e*]pyrimido[1,2-*c*][1,3]thiazine-6(2*H*)-thione (12 m): Yellow solid (528 mg, 57%).

General procedure for the synthesis of imine products: Thiazinethione **12** (1 equiv) was suspended in 0.1 M NaOH (20 mL mmol^{-1}, MeOH/H_2O = 9:1), and the mixture was stirred under reflux for 16 h. The solvent was removed under reduced pressure, and the residue was dried azeotropically with MeOH (3×20 mL mmol^{-1}) and $CHCl_3$ (2×20 mL mmol^{-1}). The solid was suspended under an argon atmosphere in dry EtOH (4 mL mmol^{-1}) and BrCN (2 equiv) was added. The mixture was stirred under reflux for 3 h, 2 M NaOH (4 mL mmol^{-1}) was added, and the solution was extracted with $CHCl_3$ (2×20 mL mmol^{-1}). The combined organic layer was dried (Na_2SO_4), and the solvent was removed under reduced pressure. The crude product was purified by column chromatography (AlO_2-N).

3,4-Dihydrobenzo[*e*]pyrimido[1,2-*c*][1,3]thiazin-6(2*H*)-imine (13 a): Colorless solid (40 mg, 10%).

2*H*-Benzo[*e*]imidazo[1,2-*c*][1,3]thiazin-5(3*H*)-imine (13 b): Colorless solid (21.2 mg, 21%).

9-Chloro-2*H*-benzo[*e*]imidazo[1,2-*c*][1,3]thiazin-5(3*H*)-imine (13 c): Colorless solid (34.7 mg, 29%).

6-Imino-*N*,*N*-dimethyl-2,3,4,6-tetrahydrobenzo[*e*]pyrimido[1,2-*c*][1,3]thiazin-9-imine (13 d): Colorless solid (32.5 mg, 41%).

10-Chloro-3,4-dihydrobenzo[*e*]pyrimido[1,2-*c*][1,3]thiazin-6(2*H*)-imine (13 e): Colorless solid (35.6 mg, 28%).

9-Fluoro-3,4-dihydrobenzo[*e*]pyrimido[1,2-*c*][1,3]thiazin-6(2*H*)-imine (13 f): Colorless solid (82.4 mg, 35%).

9-Bromo-3,4-dihydrobenzo[*e*]pyrimido[1,2-*c*][1,3]thiazin-6(2*H*)-imine (13 g): Colorless solid (89.9 mg, 30%).

8-Fluoro-3,4-dihydrobenzo[*e*]pyrimido[1,2-*c*][1,3]thiazin-6(2*H*)-imine (13 h): Colorless solid (123 mg, 53%).

7-Fluoro-2*H*-benzo[*e*]imidazo[1,2-*c*][1,3]thiazin-5(3*H*)-imine (13 i): Colorless solid (45.5 mg, 21%).

11-Bromo-3,4-dihydrobenzo[*e*]pyrimido[1,2-*c*][1,3]thiazin-6(2*H*)-imine (13 j): Pale-yellow solid (52.3 mg, 35%).

9-Methyl-3,4-dihydrobenzo[*e*]pyrimido[1,2-*c*][1,3]thiazin-6(2*H*)-imine (13 k): Colorless solid (123 mg, 28%).

10-Fluoro-3,4-dihydrobenzo[*e*]pyrimido[1,2-*c*][1,3]thiazin-6(2*H*)-imine (13 l): Colorless solid (73.3 mg, 33%).

11-Methyl-3,4-dihydrobenzo[*e*]pyrimido[1,2-*c*][1,3]thiazin-6(2*H*)-imine (13 m): Colorless solid (74.2 mg, 321 μmol, 34%).

Biological methods

Enzyme activity assays for HDACs 1, 2, 3, and 6: The activities of HDACs 1–3 and 6 were determined by a colorimetric assay as described by Wegener et al.[22] 1 nM HDAC was incubated with increasing concentrations of the respective compound for 30 min at 30 °C. The reaction was initiated by the addition of 50 μM of the substrate Boc-Lys(Ac)-AMC. After incubation for 60 min, the reaction was stopped by the addition of 20 μM suberoylanilide hydroxamic acid (SAHA, vorinostat), and the deacetylated substrate was converted into a fluorescent product by the addition of trypsin.

Enzyme activity assays for HDACs 4, 5, 7, and 8: The activities of HDACs 4, 5, 7, and 8 were determined by a colorimetric assay by using the same assay principle as that described above. The respective HDAC (1 nM) was incubated with increasing concentrations of the respective compound for 30 min at 30 °C. The reaction was initiated by the addition of 20 μM of the substrate Boc-Lys(trifluoracetyl)-AMC. After incubation for 60 min, the reaction was stopped by the addition of 20 μM 9,9,9-trifluoro-8,8-dihydroxy-*N*-phenylnonanamide (SATFMK), and the deacetylated substrate was converted into a fluorescent product by the addition of trypsin. Data were fitted by using Hill model and GraphPad Prism 6.

In vitro growth inhibition assay: SK-UT-1, a leiomyosarcoma cell line, and MCF7, a breast cancer cell line, were grown in Dulbecco modified Eagle medium (DMEM; Lonza). Jurkat, T-cell leukemia cells were grown in RPMI-1640 medium (Sigma–Aldrich). Media were supplemented with 10% heat inactivated fetal bovine serum (FBS), L-glutamine (2 mM), penicillin (100 U mL^{-1}), and streptomycin (100 μg mL^{-1}) (Lonza). Cell proliferation was monitored by using a resazurin reduction assay.[23] Each inhibitor was dissolved into DMSO (Sigma–Aldrich) and five scalar concentrations were evaluated. The different cell lines were seeded in 96-well plates (Sarstedt) at the following concentrations: 6×10^4 (SK-UT-1), 9×10^4 (Jurkat), 8×10^4 (MCF7) per 100 μL total volume. After a period of 24 h, the cells were treated with escalating doses of the different compounds. After another 40 h, resazurin solution (0.15 mg mL^{-1}, 20 μL) (Sigma–Aldrich) was added to each well and incubated at 37 °C for 150 min. The reduction of resazurin into resorufin by viable cells was quantified by using the Enspire microplate fluorimeter (PerkinElmer) equipped with a λ = 560/590 nm excitation/emission filter. For each tested compound concentration at least three different experiments with three replicates were performed. The median growth inhibition (GI_{50}) values were calculated by using GraphPad Prism.

Immunoblot analysis: Immunoblots were performed as previously described.[24] Briefly, proteins obtained after an sodium dodecyl sulfate (SDS) denaturing lysis and sonication were transferred to a 0.2 μm pore-sized nitrocellulose membrane and incubated with anti-acSMC3 (Medical and Biological Laboratories, PD040) or anti-SMC3 (Biomol, A300-0601M) antibodies. Blots were then rinsed with Blotto/Tween 20 (3×) and incubated with the relative secondary antibody (Sigma–Aldrich, Milan, Italy) for 1 h at room temperature. Blots were then washed in Blotto/Tween 20 (3×), rinsed in phosphate-buffered saline, and developed with Super Signal West Dura, as recommended by the vendor (Pierce, Rockford, IL).

Chemoinformatics

The chemical structures of the imine series were represented by 249 chemical 2D descriptors implemented in the MOE program (Chemical Computing Group Inc.). Subsequently, the relationship between the IC_{50} values against HDAC8 and the chemical structures was analyzed by a classical principal component analysis (PCA) using the same program.

Acknowledgements

F.J.M.A. was supported by the Deutsche Forschungsgemeinschaft (DFG) (grant GZ: ME 3122/2-1). Research activities in the research group of C.B. were supported by the Associazione Italiana per la Ricerca sul Cancro (AIRC) (IG-10437). E.D.G. received the Alberta Baruchello e Maurizio Scalabrin fellowship from AIRC.

Keywords: cancer · drug discovery · HDAC8 · histone deacetylase 8 · inhibitors

[1] a) C. Choudhary, C. Kumar, F. Gnad, M. L. Nielsen, M. Rehman, T. C. Walther, J. V. Olsen, M. Mann, *Science* **2009**, *325*, 834 – 840; b) T. Ouidir, P. Cosette, T. Jouenne, J. Hardouin, *Proteomics* **2015**, *15*, 2152 – 2157; c) J. D. Jones, C. D. O'Connor, *Proteomics* **2011**, *11*, 3012 – 3022; d) G.-W. Kim, X.-J. Yang, *Trends Biochem. Sci.* **2011**, *36*, 211 – 220.

[2] S. Balasubramanian, J. Ramos, W. Luo, M. Sirisawad, E. Verner, J. J. Buggy, *Leukemia* **2008**, *22*, 1026 – 1034.

[3] I. Oehme, H. E. Deubzer, D. Wegener, D. Pickert, J. P. Linke, B. Hero, A. Kopp-Schneider, F. Westermann, S. M. Ulrich, A. von Deimling, M. Fischer, O. Witt, *Clin. Cancer Res.* **2009**, *15*, 91 – 99.

[4] G. Niegisch, J. Knievel, A. Koch, C. Hader, U. Fischer, P. Albers, W. A. Schulz, *Urol. Oncol.* **2013**, *31*, 1770 – 1779.

[5] S. Y. Park, J. A. Jun, K. J. Jeong, H. J. Heo, J. S. Sohn, H. Y. Lee, C. G. Park, J. Kang, *Oncol. Rep.* **2011**, *25*, 1677 – 1681.

[6] I. Rettig, E. Koeneke, F. Trippel, W. C. Mueller, J. Burhenne, A. Kopp-Schneider, J. Fabian, A. Schober, U. Fernekorn, A. von Deimling, H. E. Deubzer, T. Milde, O. Witt, I. Oehme, *Cell Death Dis.* **2015**, *6*, e1657.

[7] *ClinicalTrials.gov* (A service of the US National Institutes of Health): clinicaltrials.gov, data retrieved on November 12, 2015.

[8] R. E. Vandenbroucke, C. Libert, *Nat. Rev. Drug Discovery* **2014**, *13*, 904 – 927.

[9] W. Tang, T. Luo, E. F. Greenberg, J. E. Bradner, S. L. Schreiber, *Bioorg. Med. Chem. Lett.* **2011**, *21*, 2601 – 2605.

[10] K. KrennHrubec, B. L. Marshall, M. Hedglin, E. Verdin, S. M. Ulrich, *Bioorg. Med. Chem. Lett.* **2007**, *17*, 2874 – 2878.

[11] L. Whitehead, M. R. Dobler, B. Radetich, Y. Zhu, P. W. Atadja, T. Claiborne, J. E. Grob, A. McRiner, M. R. Pancost, A. Patnaik, W. Shao, M. Shultz, R. Tichkule, R. A. Tommasi, B. Vash, P. Wang, T. Stams, *Bioorg. Med. Chem.* **2011**, *19*, 4626 – 4634.

[12] C. Y. Wang, L. H. Lee, *Antimicrob. Agents Chemother.* **1977**, *11*, 753 – 755.

[13] S. Shen, A. P. Kozikowski, *ChemMedChem* **2016**, *11*, 15 – 21.

[14] a) A. M. Chamoun-Emanuelli, M. Bobardt, B. Moncla, M. K. Mankowski, R. G. Ptak, P. Gallay, Z. Chen, *Antimicrob. Agents Chemother.* **2014**, *58*, 687 – 697; b) T. Mizuhara, S. Oishi, H. Ohno, K. Shimura, M. Matsuoka, N. Fujii, *Bioorg. Med. Chem.* **2012**, *20*, 6434 – 6441.

[15] M. R. Birck, T. P. Holler, R. W. Woodard, *J. Am. Chem. Soc.* **2000**, *122*, 9334 – 9335.

[16] C. A. Lipinski, F. Lombardo, B. W. Dominy, P. J. Feeney, *Adv. Drug Delivery Rev.* **2001**, *46*, 3 – 26.

[17] A. L. Hopkins, C. R. Groom, A. Alex, *Drug Discovery Today* **2004**, *9*, 430 – 431.

[18] M. D. Shultz, *Bioorg. Med. Chem. Lett.* **2013**, *23*, 5992 – 6000.

[19] T. Mizuhara, S. Oishi, N. Fujii, H. Ohno, *J. Org. Chem.* **2010**, *75*, 265 – 268.

[20] S. Okazaki, S. Oishi, T. Mizuhara, K. Shimura, H. Murayama, H. Ohno, M. Matsuoka, N. Fujii, *Org. Biomol. Chem.* **2015**, *13*, 4706 – 4713.

[21] a) T. Dasgupta, J. Antony, A. W. Braithwaite, J. A. Horsfield, *J. Biol. Chem.* **2016**, *291*, 12761 – 12770; b) M. A. Deardorff, M. Bando, R. Nakato, E. Watrin, T. Itoh, M. Minamino, K. Saitoh, M. Komata, Y. Katou, D. Clark et al., *Nature* **2012**, *489*, 313 – 317.

[22] D. Wegener, C. Hildmann, D. Riester, A. Schwienhorst, *Anal. Biochem.* **2003**, *321*, 202 – 208.

[23] U. Cersosimo, A. Sgorbissa, C. Foti, S. Drioli, R. Angelica, A. Tomasella, R. Picco, M. S. Semrau, P. Storici, F. Benedetti, F. Berti, C. Brancolini, *J. Med. Chem.* **2015**, *58*, 1691 – 1704.

[24] E. Di Giorgio, E. Gagliostro, A. Clocchiatti, C. Brancolini, *Mol. Cell. Biol.* **2015**, *35*, 1633 – 1647.

Received: October 19, 2016
Published online on ■■ ■■, 0000

*A. Kleinschek, C. Meyners, E. Digiorgio, C. Brancolini, F.-J. Meyer-Almes**

■■ – ■■

Potent and Selective Non-hydroxamate Histone Deacetylase 8 Inhibitors

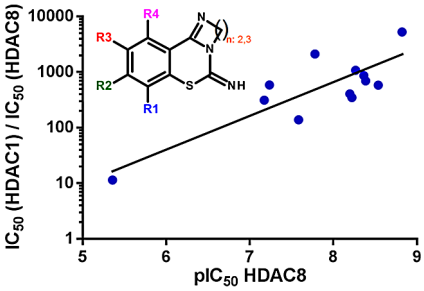

Evading traditional concepts: The pyrimido[1,2-*c*][1,3]benzothiazin-6-imine scaffold does not contain any of the common zinc(II) binding groups. Nevertheless, some derivatives of this scaffold show extraordinarily high potency and selectivity against histone deacetylase 8, an important cancer target.